




Intersublattice entanglement entropy as an extensive property in antiferromagnetsDion M. F. Hartmann ^{1,*}, Jurriaan J. Wouters,¹ Dirk Schuricht ¹, Rembert A. Duine,^{1,2,3} and Akashdeep Kamra ^{2,4}¹*Institute for Theoretical Physics, Utrecht University, Leuvenlaan 4, NL-3584 CE Utrecht, The Netherlands*²*Center for Quantum Spintronics, Department of Physics, Norwegian University of Science and Technology, NO-7491 Trondheim, Norway*³*Department of Applied Physics, Eindhoven University of Technology, P.O. Box 513, 5600 MB Eindhoven, The Netherlands*⁴*Condensed Matter Physics Center (IFIMAC) and Departamento de Física Teórica de la Materia Condensada, Universidad Autónoma de Madrid, E-28049 Madrid, Spain*

(Received 15 March 2021; accepted 19 July 2021; published 19 August 2021)

Recent advancements in our understanding of ordered magnets call for a quantification of their entanglement content on an equal footing with classical thermodynamic quantities, such as the total magnetic moment. We evaluate the entanglement entropy (EE) between the two sublattices of a bipartite ordered antiferromagnet, finding it to scale with volume. Thus, the EE density becomes an intensive property and is evaluated to be a universal dimensionality-dependent constant when exchange is the dominant interaction. Our analytic results are validated against the DMRG-based analysis of a one-dimensional (1D) system, finding good agreement. Furthermore, our evaluated EE per bond provides a useful shortcut towards obtaining the central-cut EE in 1D, and the area law in higher-dimensional magnets.

DOI: [10.1103/PhysRevB.104.064436](https://doi.org/10.1103/PhysRevB.104.064436)**I. INTRODUCTION**

Antiferromagnets (AFMs) and their different phases pervade condensed-matter physics. They underlie research fields such as spin fluctuations, mechanism of high- T_c superconductivity [1–3], and quantum spin liquids [4–8], as well as applications such as exchange-biasing in magnetic read heads [9–11]. There exists a sharp contrast between the two widespread approaches towards understanding AFMs. In the first “quantum” approach [6–8], determining the ground-state wave function for various model AFMs is a major goal. The true ground state, comprising distant entangled spins, is often not known and is complicated. Various numerical methods are employed in approximating the ground state and the excitations. The investigated system size is often limited by computational power. In the second “semiclassical” approach [12–17], a mean-field approximation is made and spatially resolved spin densities or magnetizations become classical fields within the Landau-Lifshitz description [18,19]. A Néel-ordered ground state is assumed and yields results consistent with many experiments [13,15,17,20]. Macroscopic averaging is one of the reasons why nonlocal spin correlations and entanglement, fundamental in the quantum approach, appear to not affect several experiments consistent with the semiclassical approach.

Entanglement is an important resource in quantum information and computing protocols [21–23]. Two subsystems are said to be entangled if the wave function describing the total system cannot be factored into a product of two wave functions, one for each subsystem. Furthermore, in the quantum approach discussed above, entanglement offers

a powerful metric for characterizing ground state and excitations, mapping complicated wave functions existing in very-high-dimensional space to a scalar quantity [7,24–26]. In a widely employed technique, a three-dimensional AFM is partitioned via a closed surface and the entanglement entropy (EE) between the two partitions is evaluated. The EE then bears a contribution proportional to the partition surface area, known as the area law [7,26–28]. An additional, and sometimes universal, offset in the area law probes and characterizes topology and long-range entanglement in ground and excited states of the AFM [26,29].

Recent works relate magnons with squeezed states studied in quantum optics [30–33] to demonstrate a nonzero entanglement in magnets [31–34], even in the mean-field approximation employed in the magnon-based semiclassical theory. This calls for a systematic quantification of EE as a quantum property describing such ordered magnets. We note two key motivations for this. First, the EE offers a simple scalar metric from which the proximity of a numerically evaluated ground-state wave function of an ordered state can be measured. This facilitates analysis and approximations for quantum ground states. Second, the recent breakthroughs in robust experimental control of AFMs [13,17,20] obeying the semiclassical approach outlined above pave the way for using them as a resource or battery for entanglement [26,32,35]. Such efforts benefit from adding EE to the (quantum) thermodynamic description of magnets.

In this paper, partitioning the AFM into two sublattices (Fig. 1), we establish the EE (density) as an extensive (intensive) quantum property characterizing ordered AFMs. Working within the mean-field approximation and magnon picture, we analytically evaluate the EE in the ground state, finding it to scale with the system size in the thermodynamic limit. Contradicting a preliminary expectation suggesting an

*d.m.f.hartmann@uu.nl

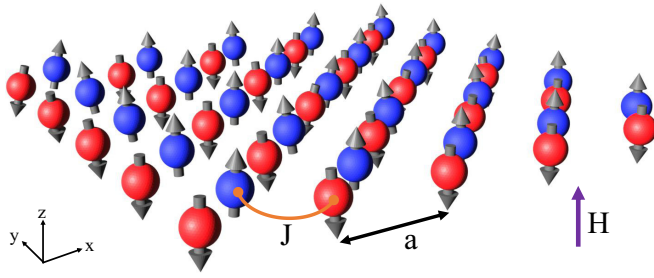


FIG. 1. The studied system for $d = 2$, $N = 5$ close to a Néel state. Sublattice A (blue) and B (red) both have an equal amount of spins. The exchange interaction (orange) is restricted to nearest neighbors and is identical for each pair of neighbors. The external magnetic field (purple) is along the z direction.

increase in EE with exchange interaction strength [31,33], the EE density is found to be a universal constant depending only on system dimensionality. This universality could offer useful benchmarking in analyzing quantum ground states. Examining its dependence on an applied magnetic field, we find that EE remains unchanged on approaching the spin-flop transition, where various classical response functions diverge [19,36].

Our analytic results are found to agree well with a density matrix renormalization group (DMRG) analysis of a one-dimensional (1D) AFM. Furthermore, our evaluated EE per bond provides an analytic shortcut to evaluating EE for the widely employed system partitioning into two spatially separated regions [26].

II. MODEL

We consider a d -dimensional uniaxial AFM in an external magnetic field along the z axis with N spins in each direction on sublattice A (B) pointing along the ($-$) z axis described by the Hamiltonian

$$\mathcal{H} = \frac{J}{\hbar^2} \sum_{i,\delta} \mathbf{S}_A(\mathbf{r}_i) \cdot \mathbf{S}_B(\mathbf{r}_i + \delta) - \sum_{\alpha \in \{A,B\}} \sum_i \left(\frac{K}{\hbar^2} [S_\alpha^{(z)}(\mathbf{r}_{i_\alpha})]^2 + \gamma H S_\alpha^{(z)}(\mathbf{r}_{i_\alpha}) \right), \quad (1)$$

with J the exchange coupling, K the anisotropy energy, δ the vectors to nearest neighbors, $\gamma < 0$ the gyromagnetic ratio, and H the external magnetic field. Our final expression for EE does not depend on the lattice or spin S considered, as long as $\sum_\delta \delta = \mathbf{0}$. Thus, for concreteness and without loss of generality, we consider a square lattice. We closely follow the derivation of Ref. [31] in this section and expand upon their results by considering all magnon modes.

Figure 1 depicts a two-dimensional system with $N = 5$ spins per sublattice per dimension. Assuming the magnetic field is below the spin-flop transition [i.e., $|\gamma|\hbar H < 2S\sqrt{K(J+K)}$], we apply a Holstein-Primakoff transformation to express the Hamiltonian in local bosonic operators a_i (b_j) which annihilate a spin flip on the i th (j th) site of the A (B) sublattice and satisfy the canonical bosonic commutation

relations [18]. We assume periodic boundary conditions. After a Fourier transform we obtain the Hamiltonian up to second order in these ladder operators assuming high S :

$$\mathcal{H} = \sum_{\mathbf{k}} A_+ a_{\mathbf{k}}^\dagger a_{\mathbf{k}} + A_- b_{\mathbf{k}}^\dagger b_{\mathbf{k}} + C_{\mathbf{k}} a_{\mathbf{k}} b_{-\mathbf{k}} + C_{\mathbf{k}}^* b_{-\mathbf{k}}^\dagger a_{\mathbf{k}}^\dagger, \quad (2)$$

$$A_\pm = JS c + 2KS \pm \gamma \hbar H, \quad C_{\mathbf{k}} = JS \sum_{\delta} e^{i\mathbf{k} \cdot \delta}. \quad (3)$$

Here, c is the coordination number and S the total spin per site. The sum over \mathbf{k} runs over the Brillouin zone, i.e., $\mathbf{k} \cdot \hat{\mathbf{e}}_i \in \{-\pi/a, \dots, \pi(N-2)/L\}$, with $L = aN$ and a the lattice spacing. It is known [37] that the eigenstate depends only on the sum $A_+ + A_- \equiv 2A$, hence the magnetic field does not affect the entanglement entropy within the Néel state approximation.

We diagonalize the Hamiltonian by applying a Bogoliubov transformation $\mathcal{H} = \sum_{\mathbf{k}} E_{\mathbf{k}}^- \alpha_{\mathbf{k}}^\dagger \alpha_{\mathbf{k}} + E_{\mathbf{k}}^+ \beta_{\mathbf{k}}^\dagger \beta_{\mathbf{k}}$ to obtain the eigenenergy

$$E_{\mathbf{k}}^\pm = \pm |\gamma| \hbar H + E_{\mathbf{k}}^0, \quad \text{with } E_{\mathbf{k}}^0 = (A^2 - C_{\mathbf{k}}^2)^{1/2} \text{ and } \alpha_{\mathbf{k}} \text{ and } \beta_{\mathbf{k}} \text{ are squeezed sublattice magnons as given in Ref. [31].}$$

Thus the ground state is squeezed [38]: Whereas a and b operate only on one sublattice, α and β operate on both. So we expect a finite entanglement in the ground state.

In Fock notation we write a state in terms of $\otimes_{\mathbf{k}} |N_{b_{\mathbf{k}}}, N_{a_{\mathbf{k}}}\rangle_{\text{sub},\mathbf{k}}$ in the sublattice basis, or in terms of $\otimes_{\mathbf{k}} |N_{\beta_{\mathbf{k}}}, N_{\alpha_{\mathbf{k}}}\rangle_{\text{sq},\mathbf{k}}$ in the squeezed basis. The product over \mathbf{k} ranges over all N^d allowed wave modes. The ground state is the squeezed vacuum $\otimes_{\mathbf{k}} |0, 0\rangle_{\text{sq},\mathbf{k}}$. We use the two-mode squeezing operator $S(r_{\mathbf{k}}) = \exp r_{\mathbf{k}}(a_{\mathbf{k}} b_{\mathbf{k}} - a_{\mathbf{k}}^\dagger b_{\mathbf{k}}^\dagger)$, with $r_{\mathbf{k}} = \text{arccosh}[(A + E_{\mathbf{k}}^0)/2E_{\mathbf{k}}^0]^{1/2}$, and exploit the Baker-Hausdorff lemma [39] to express the ground state in terms of the sublattice basis

$$|G\rangle = \otimes_{\mathbf{k}} |0, 0\rangle_{\text{sq},\mathbf{k}} = \prod_{\mathbf{k}} S(r_{\mathbf{k}}) \otimes_{\mathbf{k}} |0, 0\rangle_{\text{sub},\mathbf{k}} = \otimes_{\mathbf{k}} \frac{1}{\cosh r_{\mathbf{k}}} \sum_{l=0}^{\infty} (-\tanh r_{\mathbf{k}})^l |l, l\rangle_{\text{sub},\mathbf{k}}. \quad (4)$$

So, for each mode \mathbf{k} we have a sum over l ranging over all occupation numbers of this mode.

III. ENTANGLEMENT ENTROPY

Using the Schmidt decomposition we derive the reduced density matrix

$$\rho_A = \text{Tr}_B \rho = \sum_{\mathbf{n}} {}_B \langle \mathbf{n} | G \rangle \langle G | \mathbf{n} \rangle_B = \sum_{\mathbf{l}} {}_B \langle \mathbf{l} | G \rangle \langle G | \mathbf{l} \rangle_B = \otimes_{\mathbf{k}} \left(\sum_l \frac{\tanh^{2l} r_{\mathbf{k}}}{\cosh^2 r_{\mathbf{k}}} |l\rangle_{A,\mathbf{k}} \langle l|_{A,\mathbf{k}} \right), \quad (5)$$

where $\mathbf{n} = (n_1, n_2, \dots, n_{N^d})$ is a vector of N^d integers used to determine a pure Fock state $|\mathbf{n}\rangle_B$ on the B sublattice in the position basis, i.e., each integer n_i gives the occupancy of the i th position on the B sublattice. Similarly, \mathbf{l} is a vector used to determine a pure Fock state on the B sublattice in the momentum basis.

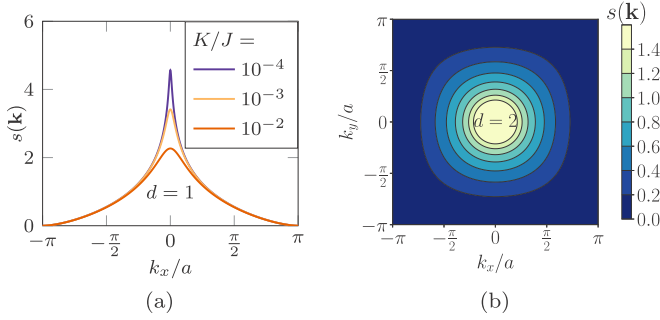


FIG. 2. The entanglement entropy per wave number $s(\mathbf{k})$ in (a) $d = 1$ and (b) $d = 2$, with $K/J = 10^{-4}$. Note that, near the Brillouin zone boundaries, the EE vanishes. Whereas in the low-wave-number regime, the EE depends approximately only on the radius of the wave vector. Thus, a smaller contribution from the high- k modes allows a low- k continuum approximation to analytically obtain the total EE.

The eigenvalues of the reduced density matrix follow immediately

$$\rho_A |\mathbf{n}\rangle_A = \lambda_{\mathbf{n}} |\mathbf{n}\rangle_A, \quad \lambda_{\mathbf{n}} = \prod_{i=1}^{N^2} \frac{\tanh^{2n_i} r_{k_i}}{\cosh^2 r_{k_i}}. \quad (6)$$

This yields an analytic expression for the EE

$$S_{EE} = - \sum_{\mathbf{n}} \lambda_{\mathbf{n}} \ln \lambda_{\mathbf{n}} = \sum_{\mathbf{k}} 2(\ln \cosh r_{\mathbf{k}} - \sinh^2 r_{\mathbf{k}} \ln \tanh r_{\mathbf{k}}). \quad (7)$$

Note that, in the sum over \mathbf{k} , all components k_i range from $-\pi/a$ to $\pi(N-2)/L$ in N steps of $2\pi/L$. The squeezing parameter $r_{\mathbf{k}}$ (and thereby the EE) does not depend on the applied external magnetic field when the magnetic field is below the spin-flop strength. Furthermore, there also is no S dependence. This result nicely extends the $k = 0$ entanglement found in Ref. [31].

For brevity we denote the term in the sum as $s(\mathbf{k})$ to investigate scaling behavior in the large- N limit

$$S_{EE} = \sum_{\mathbf{k}} s(\mathbf{k}) \approx L^d \int \frac{d^d \mathbf{k}}{(2\pi)^d} s(\mathbf{k}). \quad (8)$$

From Eq. 3 we see that the only \mathbf{k} dependence lies in $C_{\mathbf{k}}$. As Fig. 2 demonstrates for the one- and two-dimensional systems, for \mathbf{k} approaching the Brillouin zone boundary the contribution to the EE vanishes since $r_{\mathbf{k}} \rightarrow 0$.

Furthermore, note that, for small \mathbf{k} , the EE density depends mostly on the norm of \mathbf{k} . This warrants us to consider the small- \mathbf{k} limit and expand

$$\frac{|C_{\mathbf{k}}|^2}{A^2} \approx \frac{1}{\left(1 + \frac{2K}{cJ}\right)^2} \left(1 - \frac{a^2 k^2}{4}\right), \quad (9)$$

with $k^2 = \sum_{i=1}^d k_i^2$ and for the square lattice $c = 2^d$, $\delta \cdot \hat{\mathbf{e}}_i = \pm a/2$, and $C_{\mathbf{k}}$ is real. This is the only point in our derivation where details of the lattice structure enter. For instance, for a honeycomb lattice we would have $c = 3$.

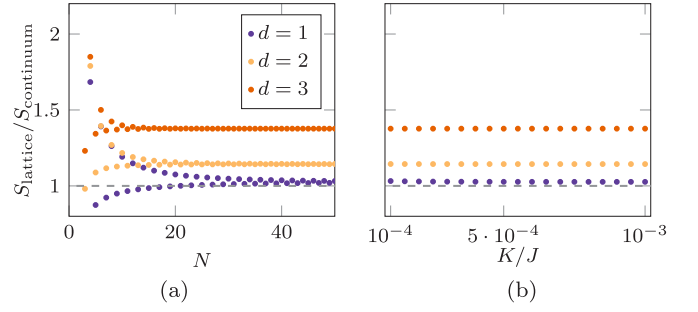


FIG. 3. The lattice entanglement entropy [Eq. 9] divided by the approximated continuum result [Eq. 10], plotted as a function of (a) the system size and (b) the ratio K/J for $N = 50$ for $d = 1$ (blue), $d = 2$ (yellow) and $d = 3$ (orange).

This demonstrates that, for $K \ll J$, our result is universal with respect to the lattice structure. Transforming the integral to spherical coordinates, leaving only the integral over the radial component k , we obtain

$$S_{EE} \approx 2^{\frac{d}{2}+1} N^d \frac{\left(1 + \frac{K}{2^{d-1}J}\right)^{d/2}}{\pi^{d/2} \Gamma\left(\frac{d}{2}\right)} I\left(d, \frac{K}{J}\right), \quad (10)$$

where Γ is the Euler gamma function and an integral representation for I is given in Appendix A where we derive analytically for $K \ll J$ that $I(d, K/J) \sim d^{-2}$.

In Fig. 3 the ratio between the lattice result from Eq. 9 and the continuum limit from Eq. 10 is plotted versus N [Fig. 3(a)] and the ratio K/J [Fig. 3(b)]. Note that the finite-size effects quickly vanish as N increases and that the EE is independent of the ratio K/J in the regime $K/J \ll 1$. The error of the continuum result increases with d because it is caused by the increasing inaccuracy of the small- \mathbf{k} approximation: As d increases, so do the degrees of freedom and higher-order products of wave numbers become relevant, which are not captured in our approximation.

IV. DENSITY MATRIX RENORMALIZATION GROUP FOR A ONE-DIMENSIONAL CHAIN

The DMRG method [40] is a versatile variational numerical tool to find the low energies and corresponding eigenstates of a strongly correlated 1D system in polynomial (in system size) time.

The DMRG method is formulated in terms of matrix product states (MPS) [41], making the EE straightforwardly accessible.

The DMRG algorithm approaches the lowest energy state by optimizing the MPS locally, alternating over all sites. It retains only the D most relevant states, selecting them based on the highest singular value of the weight s_i . Normalization of the state requires $\sum_i s_i^2 = 1$. The bond dimension $D < D_{\max}$ is set such that the weight of the discarded state is $\sum_{j>D} s_j^2 < 10^{-5}$. From the von Neumann entropy $S_{EE} = -2 \sum_{i=1}^D s_i^2 \ln(s_i)$ we see that the minimal required bond dimension is related to the EE. In contrast with the two-sublattice partitioning discussed above, the DMRG utilizes the bipartition displayed in the bottom of Fig. 4. The area law tells us that, for gapped systems,

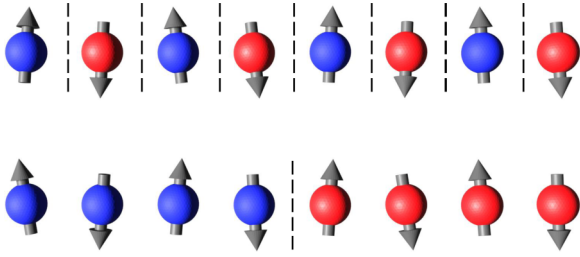


FIG. 4. For the intersublattice entanglement (top) we divide our system into two parts, red and blue, by alternating sites. For the central cut entanglement (CCEE) (bottom) we split the system through the middle. As the DMRG results suggest, the CCEE is a good approximation of the intersublattice entanglement entropy per bond.

the entanglement and thus the bond dimension is chosen independent of system length [27,28,42]. This showcases the great advantage of DMRG, requiring only linear (in N) memory allocation and polynomial computation time. The numerical results presented here are obtained with the TeNPy library [43].

The area law in 1D dictates a linear relation of the EE to the length of the cut: $S_{EE} = S_0 L_{\text{cut}}$. We recognize for the central-cut bipartition (bottom Fig. 4) $L_{\text{cut}} = 1$ and for intersublattice bipartition (top Fig. 4) $L_{\text{cut}} = 2N$. This allows us to compare the analytic intersublattice EE with the numerical CCEE. The black data in Fig. 5 confirm that the numerical CCEE matches the intersublattice EE density (no spin dependence) very well for spin $S = 3/2, 2, 5/2$ and a large range of anisotropy (K/J), moreover confirming numerically the independence of EE with respect to S . As discussed in Appendix B, the 1D spin-1 and spin-1/2 cases are not captured by the magnon approximation (for small K/J) due to dominating quantum fluctuations. We attribute the deviation in the CCEE at small $K/J < 5 \times 10^{-2}$ to the existence of low-energy modes. In this region there is either a gapless transition of a gapless phase, increasing correlations and entanglement. Specifically, for half-integer spin S the model at $K = H = 0$ is gapless by virtue of the Lieb-Schultz-Mattis theorem [44,45]. On the

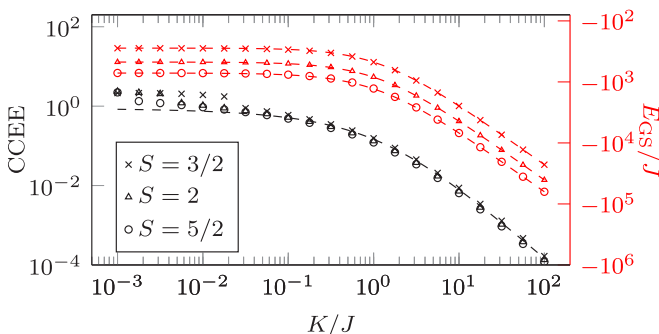


FIG. 5. Comparison of approximate analytical ground state (4) with the full DMRG ground state for $N = 50$. The marks denote the numerical results for spin 3/2 (crosses), spin 2 (triangles), and spin 5/2 (circles) with the analytical result as a dashed line. The black results compare the central-cut entanglement entropy (CCEE) for DMRG to the analytical spatial entanglement entropy density $S_{EE}/2N$. The red results compare the analytical with the numerical ground-state energy (given in Appendix C).

other hand, for $S = 2$ a phase transition was identified at [46] $K/J \approx 0.0046$. In both cases, low-energy states are present, leading to a logarithmic dependence of the CCEE on the system size [27,42].

Besides the good agreement in EE, Fig. 5 shows in red that the analytical and numerical ground-state energies match, giving yet another hint that the squeezed state provides a good representation of the low-energy physical behavior.

V. DISCUSSION

Some key features of and a comparison between our analytic and DMRG methods should be noted. In the former approach, the two-sublattice partitioning allowed us to express the total EE as a sum over \mathbf{k} [Eq. 9]. This further allowed demonstrating its scaling with system volume and obtaining analytic results [Eq. 10] via the continuum approximation. As the EE becomes small for \mathbf{k} close to the Brillouin-zone boundary, the dependence of EE on the microscopic lattice is expected to be weak, as motivated in Fig. 2(b). Thus we expect the result Eq. 9 to be valid for bipartite lattices in general, and in this sense to be universal.

Crucial to these simplifications has been our unconventional choice of the partitioning which admits translation invariance, see Fig. 1. Due to the equivalence between all nearest neighbor exchange “bonds,” the total EE per bond becomes a well-defined quantity. Thus, the area law of EE obtained with more commonly employed partitions dividing the AFM into two parts [7,26], is understood as the EE per bond times the number of bonds that the partition intersects. This is illustrated in Fig. 4. In this manner, our finding of EE being an extensive property is consistent with the area law and our choice of the partition [26,27].

Furthermore, we find that EE does not depend on the applied magnetic field and remains constant [see Eq. 8], as the system approaches the spin-flop transition from below. At this value of applied magnetic field, one of the magnon modes becomes gapless, resulting in a divergence in various response functions [19,20,36], such as the high-frequency susceptibility. Nevertheless, the EE remains well behaved and unperturbed as it is a property of the ground-state wave function, which remains unaltered on approaching this transition from below. The DMRG analysis corroborates this independence of magnetic field for the EE, see Appendix D.

Our 1D DMRG based results show a good agreement with respect to the energy and EE of the analytic squeezed ground state as displayed in Fig. 5. While the agreement between the energies is excellent, a small deviation in the EE demonstrates that it is more sensitive when comparing the quantum ground states. Quantum Monte Carlo [47] and tensor network [48] evidence for 2D antiferromagnetic Heisenberg model suggests that, for higher dimensions, the magnon approximation shows less deviation for low K/J . Furthermore, a good agreement between our analytic EE per bond and the central-cut EE for long chains suggests a shortcut in evaluating the latter, disregarding the finite-size effects.

Our methodology can be generalized to describe frustrated systems [6] starting from classically ordered states via multisublattice (three-sublattice for a triangular spin lattice [6]) models. Since finite temperature and dissipation effects en-

courage ordering, this approach offers a natural path towards accounting for these nonidealities. Besides its relevance for quantum ground states, our work clarifies the presence and nature of entanglement in a broad range of AFMs [10,17,20] adequately described via magnon theory from low to high temperatures. Our work clarifies how spins on opposite sublattices of an AFM are entangled much more strongly due to exchange, as compared with spins on the same antiferromagnetic sublattice or in a ferromagnet that derive entanglement from anisotropy [32,37]. Hence, to transfer this entanglement to external qubits, coupling them to opposite sublattices is preferred.

VI. SUMMARY

We have investigated the entanglement entropy in the ground state of an ordered antiferromagnet using a two-sublattice partitioning. The translational invariance associated with the latter enabled us to obtain analytic results, consistent with numerics, providing insights and shortcuts for characterizing the entanglement content. We obtained and demonstrate universal behavior of the entropy with respect to several external parameters, such as the specific lattice structure, anisotropy, or magnetic field. This finding helps benchmark numerically evaluated quantum ground states and guide the development of ordered antiferromagnets for useful quantum information protocols.

ACKNOWLEDGMENTS

R.A.D. and D.S. are members of the D-ITP consortium, a program of the Dutch Organization for Scientific Research (NWO) that is funded by the Dutch Ministry of Education, Culture and Science (OCW). R.A.D. and D.M.F.H. have received funding from the European Research Council (ERC) under the European Unions Horizon 2020 research and innovation programme (Grant agreement No. 725509). This work is funded by the European Research Council (ERC) and the Research Council of Norway through its Centers of Excellence funding scheme, project 262633, ‘‘QuSpin.’’ This

work is part of the research programme of the Foundation for Fundamental Research on Matter (FOM), which is part of the Netherlands Organization for Scientific Research (NWO).

APPENDIX A: CONTINUUM RESULT INTEGRAL

The analytical continuum result for the entanglement entropy involves changing the sum to an integral over the d -dimensional volume. After the small- k approximation we are left with some prefactors, given in the main text, times a one-dimensional integral over the normalized variable x given by

$$I(d, x) = \int_0^{\pi/2\sqrt{2(1+2^{1-d}x)}} dk k^{d-1} [g_k^+(d, x) \ln g_k^+(d, x) - g_k^-(d, x) \ln g_k^-(d, x)], \quad (\text{A1})$$

$$g_k^\pm(d, x) = \frac{1}{2} \left\{ \left[1 - \left(\frac{1}{1+2^{1-d}x} - k^2 \right)^2 \right]^{-1/2} \pm 1 \right\}. \quad (\text{A2})$$

For $x = K/J = 0$ and small k we approximate the integrand by $-k^{d-1} \ln(k)$ and $\pi/2\sqrt{2} \approx 1$ to obtain the proportionality $I(d, 0) \sim d^{-2}$.

APPENDIX B: SPIN 1 FOR ONE DIMENSION

The magnon approach works particularly well in the S large and/or $D > 1$ limit. Here we present the results for $S = 1$ in 1D. Despite the good correspondence for the ground-state energy in Fig. 6(a), the CCEE [also in Fig. 6(a)] clearly shows a discrepancy between the full DMRG (squares) and analytical squeeze state (dashed line) results. For $K \gg 1$ the Néel ordered phase is recovered. However, for $K \approx 1/2$ there is an Ising transition [$c = 1/2$, not directly observable in Fig. 6(a)] into a Haldane phase (lacking long-range order) [49]. The EE of 0.855 for small K is confirmed by other numerical studies [50]. The correspondence of the CCEE between the DMRG and analytical results is assumed to be a coincidence. For spin 1/2 the anisotropy term becomes trivial: $(S^{(z)})^2 \propto I$. The remaining model is simply the Heisenberg

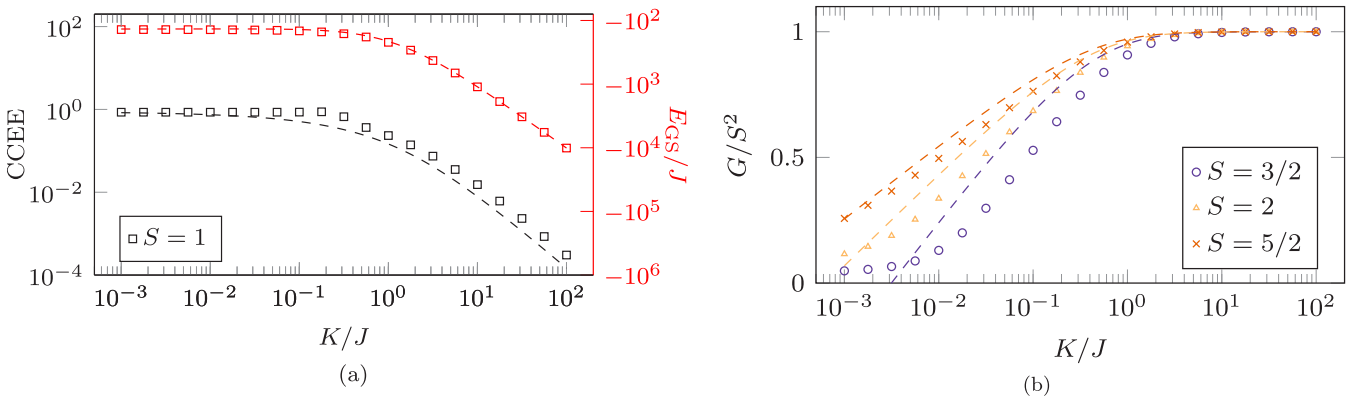


FIG. 6. (a) Comparison of approximate analytical ground state (equation 4 in the main text) with the full DMRG ground state for $N = 50$. The square marks denote the numerical results for spin 1 with the analytical result as a dashed line. The black results compare the central-cut entanglement entropy (CCEE) for DMRG to the analytical spatial entanglement entropy density $S_{EE}/2N$. The red results compare the analytical with the numerical ground-state energy. (b) Comparison of approximate analytical long-range order (G/S^2) (B1) with the full DMRG ground state for $N = 50$. The marks denote the numerical results for spin 3/2 (circles), spin 2 (triangles), and spin 5/2 (crosses) with the analytical result as a dashed line.

chain. This integrable model is critical with $c = 1$ and shows no resemblance to a magnon approximation [51]. However, this is to be expected in small S and 1D. For 2D it is known that both spin 1/2 and spin 1 exhibit Néel ordering even in the absence of anisotropy ($K = 0$) [47,48].

Analytical long-range order

The long-range correlation function, signaling (Néel) order for the squeezed ground state is

$$G = \frac{1}{2N} \sum_{j=1}^N \langle S_{A,j}^z S_{A,j+N/2}^z + S_{B,j}^z S_{B,j+N/2}^z \rangle$$

$$= \left[S - \left(\frac{1}{4\pi} \int_0^{2\pi} dk \frac{1}{\sqrt{1 - \frac{1}{(1+K/J)^2} \cos(k)^2}} - \frac{1}{2} \right) \right]^2. \quad (\text{B1})$$

This compares qualitatively to the DMRG results, as we see in Fig. 6(b). The discrepancy is to be expected, because the squeezed states are built on the ansatz of high long-range order. The low- K/J numerical behavior is explained by the vicinity of a transition or gapless region.

APPENDIX C: ANALYTICAL GROUND-STATE ENERGY

The ground-state energy of the analytical squeezed ground state is

$$E_{\text{GS}} = -\frac{JS^2 Nc}{4} - KNS^2 - \frac{(JSc + 2K)N}{4} \times \left[1 - G\left(\frac{JSc}{JSc + 2K}\right) \right], \quad (\text{C1})$$

with the elliptical integral

$$G(a) = \int_0^{2\pi} \frac{dq}{2\pi} \sqrt{1 - a^2 \cos^2 q}. \quad (\text{C2})$$

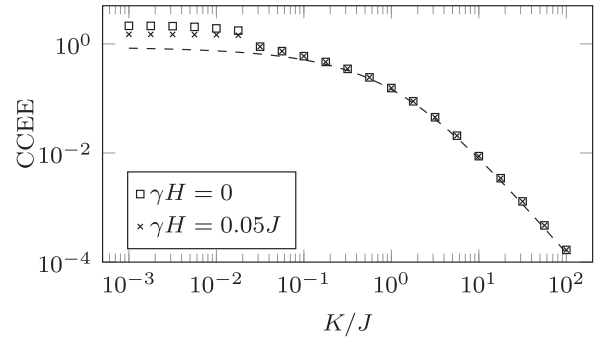


FIG. 7. The central cut entanglement entropy for $S = 3/2$, $N = 50$ and a range of K , with magnetic field (crosses $\gamma H = 0.05J$) and without (squares). For $K < 0.3J$, as described in Sec. IV, the system is not in the magnon phase but enters a critical regime. For the former, we see no dependence on magnetic field, while for the latter, there is a deviation when introducing γH .

This is the energy used in Fig. 5 in the main text against which are compared the DMRG results.

APPENDIX D: MAGNETIC-FIELD INDEPENDENCE IN ONE DIMENSION

With DMRG we investigate the magnetic-field dependence explicitly. As an example we look at spin 3/2 with and without magnetic field γH , as defined in Eq. (1). In Fig. 7 we show the CCEE for $\gamma H = 0$ and $\gamma H = 0.05J$. This value is chosen such that the system is below the spin-flop transition for all K plotted here. For $K > 0.3J$ there is no magnetic-field dependence, as expected from the magnon approximation. In Sec. IV we concluded that, for small $K < 0.3J$, the system shows critical behavior and is not described by the magnon phase. The energy dependence for small K is another indicator that we have left the magnon regime.

- [1] T. Moriya and K. Ueda, Spin fluctuations and high temperature superconductivity, *Adv. Phys.* **49**, 555 (2000).
- [2] T. Moriya and K. Ueda, Antiferromagnetic spin fluctuation and superconductivity, *Rep. Prog. Phys.* **66**, 1299 (2003).
- [3] P. A. Lee, N. Nagaosa, and X.-G. Wen, Doping a Mott insulator: Physics of high-temperature superconductivity, *Rev. Mod. Phys.* **78**, 17 (2006).
- [4] T. Itou, A. Oyamada, S. Maegawa, and R. Kato, Instability of a quantum spin liquid in an organic triangular-lattice antiferromagnet, *Nat. Phys.* **6**, 673 (2010).
- [5] T.-H. Han, J. S. Helton, S. Chu, D. G. Nocera, J. A. Rodriguez-Rivera, C. Broholm, and Y. S. Lee, Fractionalized excitations in the spin-liquid state of a kagome-lattice antiferromagnet, *Nature (London)* **492**, 406 (2012).
- [6] L. Balents, Spin liquids in frustrated magnets, *Nature (London)* **464**, 199 (2010).
- [7] L. Savary and L. Balents, Quantum spin liquids: A review, *Rep. Prog. Phys.* **80**, 016502 (2017).
- [8] C. Castelnovo, R. Moessner, and S. L. Sondhi, Spin liquids in frustrated magnets, *Nature (London)* **451**, 42 (2008).
- [9] W. Zhang and K. M. Krishnan, Epitaxial exchange-bias systems: From fundamentals to future spin-orbitronics, *Mater. Sci. Eng., R* **105**, 1 (2016).
- [10] P. Manna and S. Yusuf, Two interface effects: Exchange bias and magnetic proximity, *Phys. Rep.* **535**, 61 (2014).
- [11] J. Nogués and I. K. Schuller, Exchange bias, *J. Magn. Magn. Mater.* **192**, 203 (1999).
- [12] T. L. Gilbert, A phenomenological theory of damping in ferromagnetic materials, *IEEE Trans. Magn.* **40**, 3443 (2004).
- [13] V. Baltz, A. Manchon, M. Tsoi, T. Moriyama, T. Ono, and Y. Tserkovnyak, Antiferromagnetic spintronics, *Rev. Mod. Phys.* **90**, 015005 (2018).
- [14] E. V. Gomonay and V. M. Loktev, Spintronics of antiferromagnetic systems (review article), *Low Temp. Phys.* **40**, 17 (2014).
- [15] O. Gomonay, V. Baltz, A. Brataas, and Y. Tserkovnyak, Antiferromagnetic spin textures and dynamics, *Nat. Phys.* **14**, 213 (2018).
- [16] A. Kamra, R. E. Troncoso, W. Belzig, and A. Brataas, Gilbert damping phenomenology for two-sublattice magnets, *Phys. Rev. B* **98**, 184402 (2018).

- [17] T. Jungwirth, X. Marti, P. Wadley, and J. Wunderlich, Antiferromagnetic spintronics, *Nat. Nanotechnol.* **11**, 231 (2016).
- [18] T. Holstein and H. Primakoff, Field dependence of the intrinsic domain magnetization of a ferromagnet, *Phys. Rev.* **58**, 1098 (1940).
- [19] A. Akhiezer, V. Bar'iakhtar, and S. Peletminski, *Spin Waves* (North-Holland Publishing Company, Amsterdam, 1968).
- [20] R. Lebrun, A. Ross, S. A. Bender, A. Qaiumzadeh, L. Baldrati, J. Cramer, A. Brataas, R. A. Duine, and M. Kläui, Tunable long-distance spin transport in a crystalline antiferromagnetic iron oxide, *Nature (London)* **561**, 222 (2018).
- [21] T. C. Ralph, Continuous variable quantum cryptography, *Phys. Rev. A* **61**, 010303(R) (1999).
- [22] Z. Y. Ou, S. F. Pereira, H. J. Kimble, and K. C. Peng, Realization of the Einstein-Podolsky-Rosen Paradox for Continuous Variables, *Phys. Rev. Lett.* **68**, 3663 (1992).
- [23] F. Furrer, T. Franz, M. Berta, A. Leverrier, V. B. Scholz, M. Tomamichel, and R. F. Werner, Continuous Variable Quantum Key Distribution: Finite-Key Analysis of Composable Security Against Coherent Attacks, *Phys. Rev. Lett.* **109**, 100502 (2012).
- [24] T. Nishioka, Entanglement entropy: Holography and renormalization group, *Rev. Mod. Phys.* **90**, 035007 (2018).
- [25] R. Islam, R. Ma, P. M. Preiss, M. E. Tai, A. Lukin, M. Rispoli, and M. Greiner, Measuring entanglement entropy in a quantum many-body system, *Nature (London)* **528**, 77 (2015).
- [26] L. Amico, R. Fazio, A. Osterloh, and V. Vedral, Entanglement in many-body systems, *Rev. Mod. Phys.* **80**, 517 (2008).
- [27] P. Calabrese and J. Cardy, Entanglement entropy and conformal field theory, *J. Phys. A: Math. Theor.* **42**, 504005 (2009).
- [28] J. Eisert, M. Cramer, and M. B. Plenio, Colloquium: Area laws for the entanglement entropy, *Rev. Mod. Phys.* **82**, 277 (2010).
- [29] A. Kitaev and J. Preskill, Topological Entanglement Entropy, *Phys. Rev. Lett.* **96**, 110404 (2006).
- [30] A. Kamra and W. Belzig, Super-Poissonian Shot Noise of Squeezed-Magnon Mediated Spin Transport, *Phys. Rev. Lett.* **116**, 146601 (2016).
- [31] A. Kamra, E. Thingstad, G. Rastelli, R. A. Duine, A. Brataas, W. Belzig, and A. Sudbo, Antiferromagnetic magnons as highly squeezed Fock states underlying quantum correlations, *Phys. Rev. B* **100**, 174407 (2019).
- [32] J. Zou, S. K. Kim, and Y. Tserkovnyak, Tuning entanglement by squeezing magnons in anisotropic magnets, *Phys. Rev. B* **101**, 014416 (2020).
- [33] A. Kamra, W. Belzig, and A. Brataas, Magnon-squeezing as a niche of quantum magnonics, *Appl. Phys. Lett.* **117**, 090501 (2020).
- [34] H. Y. Yuan, S. Zheng, Z. Ficek, Q. Y. He, and M.-H. Yung, Enhancement of magnon-magnon entanglement inside a cavity, *Phys. Rev. B* **101**, 014419 (2020).
- [35] D. D. Awschalom, C. H. R. Du, R. He, F. J. Heremans, A. Hoffmann, J. T. Hou, H. Kurebayashi, Y. Li, L. Liu, V. Novosad, J. Sklenar, S. E. Sullivan, D. Sun, H. Tang, V. Tiberkevich, C. Trevillian, A. W. Tsen, L. R. Weiss, W. Zhang, X. Zhang, L. Zhao, and C. W. Zollitsch, Quantum engineering with hybrid magnonics systems and materials, [arXiv:2102.03222](https://arxiv.org/abs/2102.03222).
- [36] O. Johansen and A. Brataas, Spin pumping and inverse spin Hall voltages from dynamical antiferromagnets, *Phys. Rev. B* **95**, 220408(R) (2017).
- [37] A. Kamra, U. Agrawal, and W. Belzig, Noninteger-spin magnonic excitations in untextured magnets, *Phys. Rev. B* **96**, 020411(R) (2017).
- [38] C. Gerry, P. Knight, and P. L. Knight, *Introductory Quantum Optics* (Cambridge University Press, Cambridge, 2005).
- [39] J. J. Sakurai and E. D. Commins, *Modern Quantum Mechanics, Revised Edition* (American Association of Physics Teachers, London, 1995), p. 92.
- [40] S. R. White, Density-matrix algorithms for quantum renormalization groups, *Phys. Rev. B* **48**, 10345 (1993).
- [41] U. Schollwöck, The density-matrix renormalization group in the age of matrix product states, *Ann. Phys. (NY)* **326**, 96 (2011).
- [42] P. Calabrese and J. Cardy, Entanglement entropy and quantum field theory, *J. Stat. Mech.* (2004) P06002.
- [43] J. Hauschild and F. Pollmann, Efficient numerical simulations with tensor networks: Tensor network python (tenpy), *SciPost Phys. Lect. Notes* **5**, 5 (2018).
- [44] E. Lieb, T. Schultz, and D. Mattis, Two soluble models of an antiferromagnetic chain, *Ann. Phys. (NY)* **16**, 407 (1961).
- [45] H. Tasaki, *Physics and Mathematics of Quantum Many-Body Systems* (Springer, Cham, 2020).
- [46] J. A. Kjäll, M. P. Zaletel, R. S. K. Mong, J. H. Bardarson, and F. Pollmann, Phase diagram of the anisotropic spin-2 XXZ model: Infinite-system density matrix renormalization group study, *Phys. Rev. B* **87**, 235106 (2013).
- [47] M. Matsumoto, C. Yasuda, S. Todo, and H. Takayama, Ground-state phase diagram of quantum Heisenberg antiferromagnets on the anisotropic dimerized square lattice, *Phys. Rev. B* **65**, 014407 (2001).
- [48] H. H. Zhao, C. Xu, Q. N. Chen, Z. C. Wei, M. P. Qin, G. M. Zhang, and T. Xiang, Plaquette order and deconfined quantum critical point in the spin-1 bilinear-biquadratic Heisenberg model on the honeycomb lattice, *Phys. Rev. B* **85**, 134416 (2012).
- [49] M. den Nijs and K. Rommelse, Preroughening transitions in crystal surfaces and valence-bond phases in quantum spin chains, *Phys. Rev. B* **40**, 4709 (1989).
- [50] F. Pollmann, A. M. Turner, E. Berg, and M. Oshikawa, Entanglement spectrum of a topological phase in one dimension, *Phys. Rev. B* **81**, 064439 (2010).
- [51] T. Giamarchi, *Quantum Physics in One Dimension* (Clarendon Press, Oxford, 2003), Vol. 121.